




Recycling Molybdenum Oxides from Waste Molybdenum Disilicides: Oxidation Experimental Study and Photocatalytic Properties

Ge Kong¹ · Xiaoni Du¹ · Xiaoping Cai¹ · Peizhong Feng¹  · Xiaohong Wang¹ · Farid Akhtar²

Received: 29 December 2018 / Revised: 3 April 2019 / Published online: 16 April 2019
© Springer Science+Business Media, LLC, part of Springer Nature 2019

Abstract

To recycle elemental molybdenum from waste molybdenum disilicide (MoSi_2) heating elements, the MoSi_2 was first disintegrated to MoO_3 and SiO_2 powders in air at a pest oxidation temperature of 500 °C. X-ray diffraction (XRD) patterns confirmed the completion of the pest oxidation reaction. The mixture of MoO_3 and SiO_2 powders were heated to 950 °C in a tube furnace to evaporate MoO_3 , and the XRD patterns of the residue showed that only SiO_2 was left in the crucible, confirming that the MoO_3 was removed through thermal evaporation. The collected MoO_3 crystals had a striped morphology. Photocatalytic performance of MoO_3 showed superior activity in comparison with commercial MoO_3 and P25 for the degradation of methylene blue under visible light irradiation. The photocatalytic degradation activity of MoO_3 synthesized by thermal evaporation at 950 °C was 99.25% in 60 min.

Keywords Oxidation · Waste MoSi_2 · Recycling MoO_3 · Thermal evaporation · Photocatalytic properties

Introduction

Molybdenum disilicide (MoSi_2) is an intermetallic compound widely used in oxidizing environments at high temperature [1]. The most important commercial application of MoSi_2 is its use as heating elements in industrial furnaces. MoSi_2 heating elements can be used in air and protective gas atmospheres to heat furnaces to high temperatures [2, 3]. Typically, the lifetime of the heating elements is 3–6 years,

✉ Peizhong Feng
fengroad@163.com

¹ School of Materials Science and Engineering, China University of Mining and Technology, Xuzhou 221116, China

² Division of Materials Science, Luleå University of Technology, Luleå 97187, Sweden

depending on the furnace heating practices. With the rapid development of high-temperature process, MoSi₂ heating elements have been introduced into the glass industry, heat treatment, forging, ceramics and research and development industries [4, 5]. Although MoSi₂ heating elements exhibit excellent life, the replacement is required due to (1) the increase in resistance over the time of use because of thickening of the surface silicon oxide, (2) the damage of oxide layer as a result of long-time erosion, volatilization and formation of micro-cracks in thermal cycling, or exposure to reducing atmospheres [6]. A large amount of waste MoSi₂ has become available; however, to the best of our knowledge, the disposal of the waste MoSi₂ and/or its recycling has been reported rarely in the literature.

MoSi₂ is regarded as high-temperature structural material and generally used as heating elements. Nevertheless, MoSi₂ undergoes accelerated oxidation at 400–600 °C and is disintegrated into powder. The phenomenon is termed as pest oxidation, which was first reported by Fitzer in 1955 [7–9]. In the past few decades, many researchers have studied the low-temperature oxidation behavior of MoSi₂ and MoSi₂-based composites [10–17]. Yanagihara et al. [18] found that MoSi₂ underwent severe oxidation corrosion and was decomposed into MoO₃ and SiO₂ rapidly at 500 °C. Moreover, Chou et al. [19] reported that the pest oxidation products consisted of SiO₂ clusters and MoO₃ whiskers. Westbrook et al. [20] elucidated the mechanism of pest oxidation, and they reported that the preferential intergranular diffusion of oxygen contributed to the embrittlement of grain boundary. However, in this work, the pest oxidation was applied for the chemical separation of Mo and Si elements from the waste MoSi₂ in forms of MoO₃ and SiO₂, respectively.

Molybdenum trioxide (MoO₃) is a well-known n-type wide band gap (2.39–2.90 eV) semiconductor, which has found attractive prospects in photocatalysis [21–23]. Chithambararaj et al. [24] synthesized hexagonal molybdenum oxide (h-MoO₃) nanocrystals with a flower-like hierarchical structure and studied the photocatalytic degradation of methylene blue (MB) under irradiation of visible or UV light. Kumar et al. [25] synthesized thermodynamically stable α-MoO₃ nanoplates which exhibited strong photocatalytic degradation of MB and Rh-B up to 99% in the presence of sun light without using any oxidizing agents. A number of techniques have been reported for the deposition of MoO₃ including pulse laser deposition [26], thermal evaporation [27], sputtering [28], sol–gel [29], spray pyrolysis [21], chemical vapor deposition [30, 31] and electrodeposition [32]. Zhou et al. [27] prepared orthorhombic MoO₃ nanowires by thermal evaporation and oxidation without using any catalyst, and they found the stability of the emission current over time was within 10%, which indicated that MoO₃ nanowires could be used as a cold cathode. Rahmani et al. [22] investigated the structural and gas sensing properties of MoO₃ thin films which were prepared by thermal evaporation of MoO₃ on the gold interdigital fingers on quartz substrates. Thermal evaporation is an advantageous method for producing highly crystalline and stratified structures [22] so that it was used to separate MoO₃ from SiO₂.

In the present work, a simple and low-cost method, pest oxidation followed by thermal evaporation, for recycling of MoO₃ from waste MoSi₂ was investigated. The MoO₃ was recovered effectively to realize the recycling of Mo from wasted MoSi₂ heating elements. The process is effective for resource, environment and economy, and

the photocatalytic performance of MoO_3 for degradation of organic dyes in the water would be discussed.

Experimental Procedures

Preparation of MoO_3

Figure 1 shows the illustration of recycling of MoO_3 . The waste MoSi_2 heating element was broken in the jaw crusher and ground into powder in the roller ball mill for 24 h with a mean particle size of about $1.4 \mu\text{m}$. The waste MoSi_2 powder was weighed (m_0) before calcination, then calcined in tube furnace with a heating rate of $10 \text{ }^\circ\text{C}/\text{min}$ and held for 180 min in air at $450\text{--}550 \text{ }^\circ\text{C}$. After calcination, the oxidized powders were cooled down to room temperature naturally and weighed as m_T ($T=450 \text{ }^\circ\text{C}$, $475 \text{ }^\circ\text{C}$, $500 \text{ }^\circ\text{C}$, $525 \text{ }^\circ\text{C}$ and $550 \text{ }^\circ\text{C}$), and the mass gain (M) of powder was calculated using Eq. (1):

$$M = (m_T - m_0) / m_0 \times 100\% \quad (1)$$

Besides, the effect of holding time was explored under the similar conditions with oxidation of $500 \text{ }^\circ\text{C}$ for 30–210 min, the weight of powder after calcination was weighed as m_t ($t=30 \text{ min}$, 60 min , 90 min , 120 min , 150 min , 180 min and 210 min) and the mass gain (M) of powder was calculated by Eq. (2):

$$M = (m_t - m_0) / m_0 \times 100\% \quad (2)$$

The oxidation reaction of MoSi_2 powder calcined in the air is indicated by Eq. (3) [19, 20]:

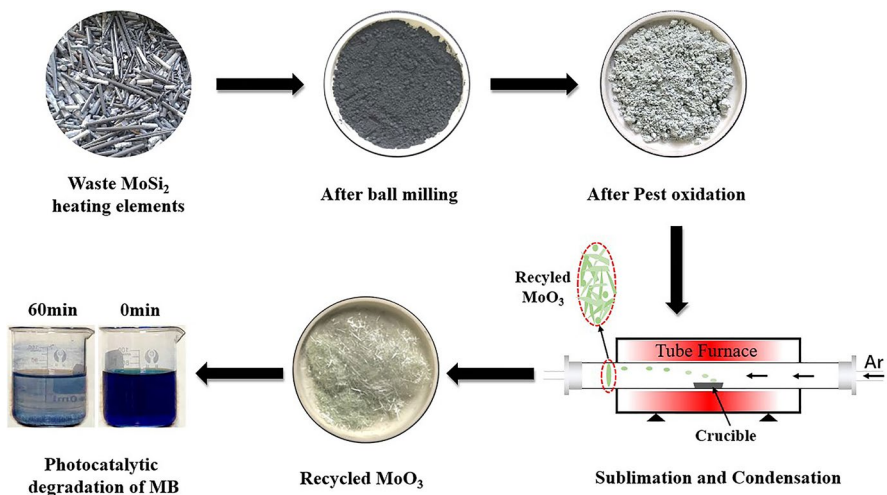
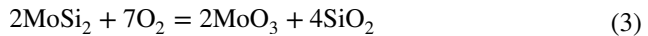


Fig. 1 Illustration of recycling and resuing of MoO_3 from waste MoSi_2 heating element

Equation (3) shows that the oxidation results in formation of MoO_3 and SiO_2 .

After calcination process, the oxidized powders were put in the crucible which was placed in the tube furnace, and the powder was heated to different temperatures (700–950 °C) at a heating rate of 8 °C/min and held for 2 h before furnace cooling. The MoO_3 was evaporated from the mixture of MoO_3 and SiO_2 , transported with flowing argon in tube furnace and collected at the glass substrate placed where the temperature gradient was high, which was marked with red circle dash lines in Fig. 1. To figure out the effect of temperature on the amount of MoO_3 evaporated, the powder was weighed and the mass loss of powder was calculated after thermal evaporation cycle.

The quantitative elemental analysis of waste MoSi_2 , recycled products and residue after thermal evaporation was performed using X-ray fluorite spectroscopy (XRF, S8 TIGER). The phase composition of recycled MoO_3 was determined by X-ray diffraction (XRD) on a Bruker D8 Advance machine with Cu target. The microstructures were characterized by scanning electron microscopy (SEM, SU8220).

Photocatalytic Performance of MoO_3

Photocatalytic experiments were carried out to degrade methylene blue (MB) in a photocatalyst aqueous suspension system, which was exposed to visible light. The initial concentration of MB was 20 mg/L. The solution containing photocatalysts was stirred in the dark for 30 min to establish a relative adsorption–desorption equilibrium between photocatalyst powders and MB solution. The photocatalytic degradation was conducted in a 50-ml glass vessel, and a 150 W halogen tungsten lamp was located 20 cm above the surface of the liquid. During irradiation, 6 ml mixture solution was withdrawn at every 10-min intervals and then centrifuged to separate photocatalysts from the mixture solution. The photocatalytic performance experiments of commercial MoO_3 (10 μm , 99.9%, purity), nano- TiO_2 (P25) were conducted under the same conditions as a comparison.

Results and Discussion

Characterization of Waste MoSi_2

The chemical composition of the waste MoSi_2 powder determined by XRF in Table 1 shows that Mo and Si are the main components; O, W, and Al are present as major impurities. Feng et al. [1] reported that Mo, W and Si powders were mixed at a molar ratio of 1:2 [(Mo + W):Si] and 2.5 at.% and 5.5 at.% of Al were introduced into Mo–W–Si powders to improve the hardness, flexural strength and fracture toughness

Table 1 Composition of waste MoSi_2 from XRF (wt%)

Element	Mo	Si	O	W	Al	Rh	Se	Fe	Mg
wt%	45.78	28.05	13.00	8.17	2.16	0.53	0.36	0.17	0.12

of MoSi_2 . The commercial Kanthal Super 1900 silicide contains tungsten, and Kanthal Super ER silicide comprises aluminum [33]. The addition of aluminum formed a thicker alumina scale at higher temperatures on Kanthal Super ER to protect the heating elements from corrosive reactions. Furthermore, during the shaping, silicide powders were mixed with clay binder to prepare MoSi_2 -base heating elements [33]. Thus, the presence of impurities, O, W, Al, largely depends on the processing of MoSi_2 heating elements.

Effects of Oxidation Temperature and Holding Time

The effect of calcination temperature on the mass gain of waste MoSi_2 powder in Fig. 2 shows that MoSi_2 oxidizes rapidly at 450–550 °C [10, 11]. The mass gain of powder reaches the maximum of 63.8% at 500 °C, which means that the MoSi_2 powder has undergone the most serious pest oxidation [11]. Above 500 °C, the mass gain decreases, which can be related to the formation of protective glass scale on the surface of material hindering the pest oxidation [6, 8–11].

Figure 3 presents the XRD patterns of waste MoSi_2 powder calcined at 450 °C, 475 °C, 500 °C, 525 °C and 550 °C for 3 h. MoO_3 was identified as the major crystalline phase; besides, unreacted MoSi_2 peaks were detected after calcination. As such, the waste MoSi_2 heating element powders can be used as a source of MoO_3 for recycling. Just as the effect of calcination temperature on mass gain is exhibited in Fig. 2, MoSi_2 powder is suffered from the most accelerated oxidation at 500 °C which corresponded to the maximum mass gain. It is evident from Figs. 2 and 3 that the calcination temperature of 500 °C is sufficiently high to transform MoSi_2 to MoO_3 as proposed by Eq. (3) by pest oxidation process.

Figure 4 shows the effect of holding time on the mass gain of waste MoSi_2 powder calcined at 500 °C. When the holding time is between 30 and 90 min, the mass gain of calcined powder increases quickly, reaching 62.1% from 50.6%;

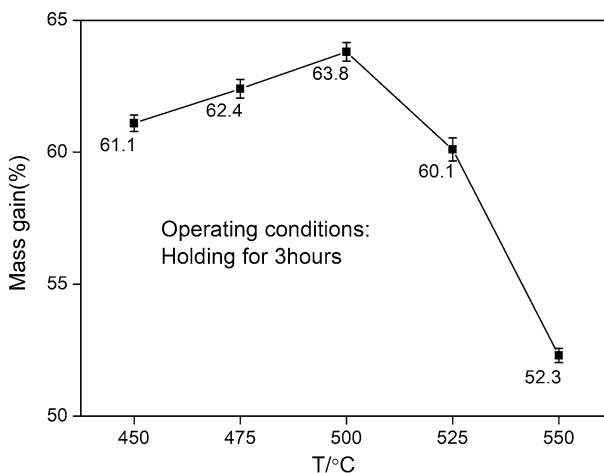


Fig. 2 Effect of calcined temperature on mass gain of waste MoSi_2 powder

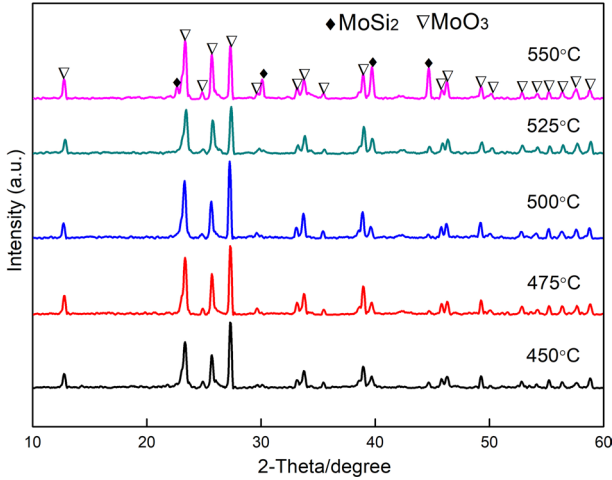


Fig. 3 XRD patterns of oxidation products of waste MoSi_2

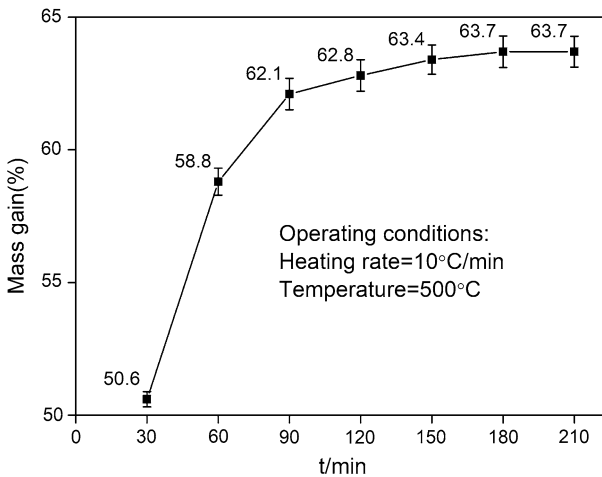


Fig. 4 Effect of holding time on mass gain of waste MoSi_2

with the prolonged holding time, it increases to 63.7% when holding for 210 min, which indicates that the extended holding time promotes the transformation of MoSi_2 into MoO_3 and SiO_2 . After calcination for 180 min, the oxidation reaction of MoSi_2 was completed and mass gain does not change with the increase in holding time.

Figure 5 shows SEM micrograph of waste MoSi_2 powder and the oxidized products calcined at 500 °C for 30 min, 120 min and 180 min. The waste MoSi_2 powder consists of particles of 1–4 μm (Fig. 5a). It can be seen that when calcined at 500 °C for 30 min, the oxidized mixture is composed of needle-shaped MoO_3 with 20 μm length and disintegrative SiO_2 particle clusters. With the holding time

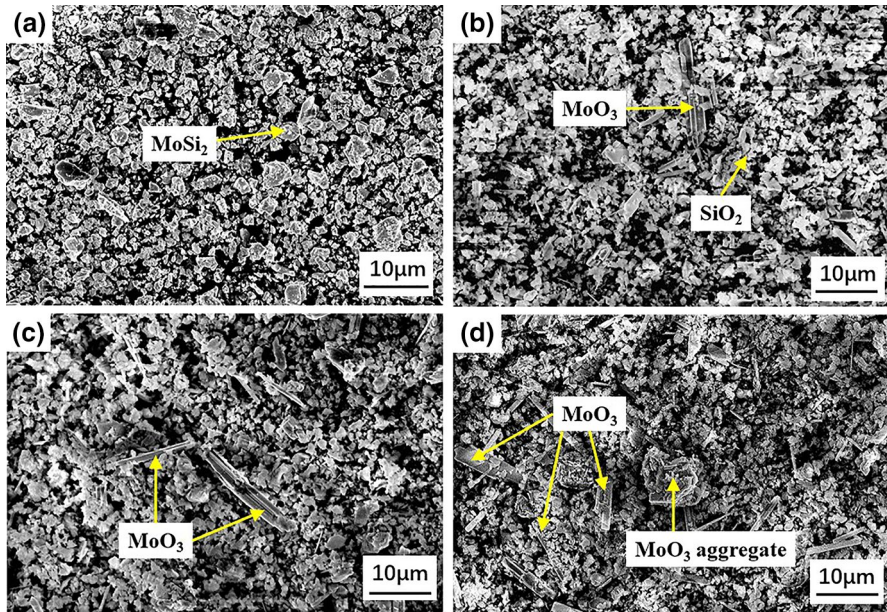


Fig. 5 SEM photographs of **a** waste MoSi_2 powder and calcined at $500\text{ }^\circ\text{C}$ for **b** 30 min, **c** 120 min and **d** 180 min

prolonged, the number of MoO_3 rods significantly increases and some rods stack together to form MoO_3 aggregates when calcined for 180 min, as can be seen in Fig. 5d.

Effect of Sublimation Temperature

Table 2 exhibits the relationship between vapor pressure of MoO_3 and temperature [34]. The vapor pressure increases as temperature rises, which climbs rapidly from 0.008 to 0.2333 kPa and 1.3467 kPa, respectively at $720\text{ }^\circ\text{C}$, $750\text{ }^\circ\text{C}$ and $800\text{ }^\circ\text{C}$. This suggests that the temperature higher than $750\text{ }^\circ\text{C}$ can volatilize MoO_3 by evaporation from the $\text{MoO}_3\text{-SiO}_2$ powder mixture.

Figure 6 presents the effect of holding temperature on the evaporated mass of MoO_3 , which increases from 31.7 to 50.2% with the temperature range from $700\text{ }^\circ\text{C}$ to $900\text{ }^\circ\text{C}$, respectively. As temperature increases to $900\text{ }^\circ\text{C}$, the evaporated mass increases. After $900\text{ }^\circ\text{C}$, the evaporated mass is stable and hits its maximum at 50.4% at $950\text{ }^\circ\text{C}$. Inset

Table 2 Relationship between vapor pressure of MoO_3 and temperature [34]

$T\text{ (}^\circ\text{C)}$	600	625	650	720	750	800	850	900	950	1000
P (kPa)	0	0.0024	0.0067	0.008	0.2333	1.347	3.12	9.526	17.547	26.506

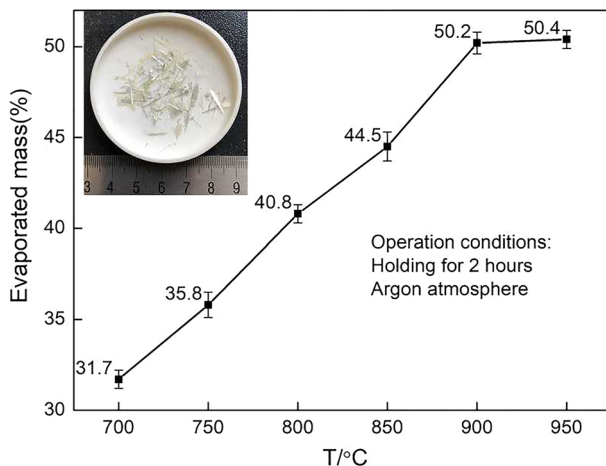


Fig. 6 Effect of temperature on the mass loss of pest oxidation products of waste MoSi_2 powder

image in Fig. 6 presents the macrograph of recycled MoO_3 recovered at 950 °C, and the recycled MoO_3 shows transparent elongated strips of size of 2–10 mm.

Figure 7 shows the XRD patterns of recycled products and the residue, and only single-phase MoO_3 is identified regardless of the heating temperature (Fig. 7a). No other diffraction peaks are present. Figure 7b demonstrates the XRD patterns of residual products in the crucible after evaporation procedure. When heating at 700 °C and 800 °C, the crystalline phases are SiO_2 and MoO_3 in the crucible, suggesting that MoO_3 has not volatilized completely. With the increase in temperature to 900 °C, the SiO_2 peaks become the strongest, and single-phase SiO_2 is found after heating at 950 °C. The XRD in Fig. 7 confirms the removal of MoO_3 from the mixture of MoO_3 and SiO_2 by thermal evaporation process.

Photocatalytic Performance

As shown in Fig. 8, the optical properties of recycled MoO_3 and commercial MoO_3 were characterized by UV–Vis diffuse reflectance spectroscopy (DRS). The optical absorption performance of semiconductors is evaluated on the basis of the band gap energy (E_g) as calculated by Eq. (4) [35]:

$$\alpha h\nu = A(h\nu - E_g)^{n/2} \quad (4)$$

In Eq. (4), α , h , ν , A and E_g represent the absorption coefficient near absorption edge, Planck constant (unit: eV), the light frequency, the absorption constant and the absorption band gap energy, respectively [35]. The value of n is determined by the type of optical transition in the semiconductor ($n=1$ for direct transition and $n=4$ for indirect transition). According to previous reports, MoO_3 pertains to direct transition and the value of n is set as 1 [35]. The Tauc plot of the corresponding samples is shown in the inset of Fig. 8, and the band gap energies of recycled MoO_3

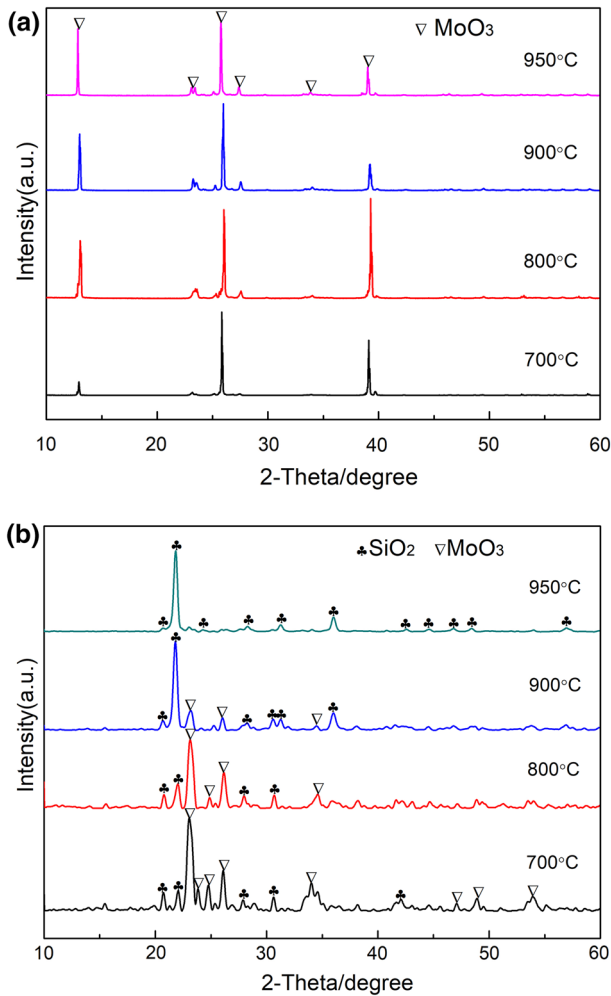


Fig. 7 XRD pattern of **a** recycled products and **b** residue after thermal evaporation at different temperatures

and commercial MoO_3 are 2.95 eV and 3.10 eV, respectively. As is shown, the band gap energy of the recycled MoO_3 is narrower than that of commercial MoO_3 , and the narrower band gap energy helps improve the photocatalytic property of MoO_3 . Furthermore, some other characterization such as photoluminescence spectra (PL), surface area and defect will be used to deeply explore the photocatalysis mechanism in the following researches.

Figure 9 exhibits the photocatalytic performance of nano- TiO_2 (P25), commercial MoO_3 (10 μm , 99.9% purity) and recycled MoO_3 at 950 °C, which was evaluated by the degradation of methylene blue (MB) under visible light irradiation. The MB degradation efficiency (%) was calculated by Eq. (5) [36]:

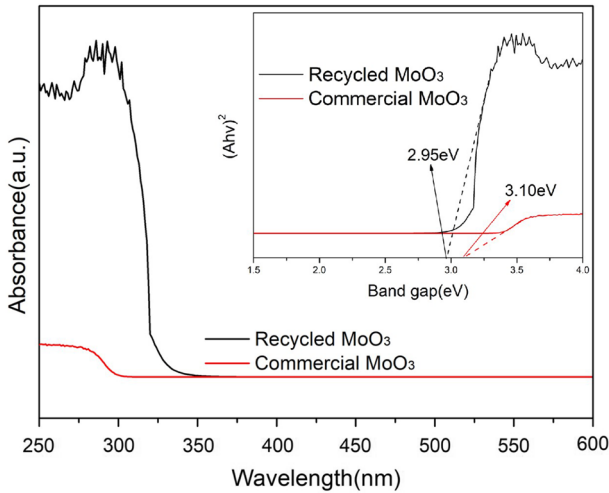


Fig. 8 UV–Vis diffuse reflectance spectra (DRS) of recycled MoO_3 and commercial MoO_3

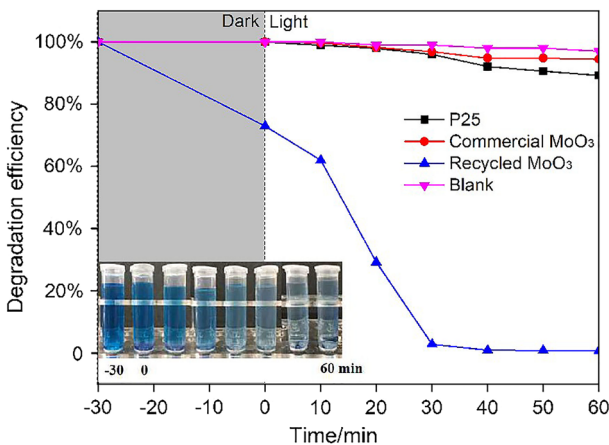


Fig. 9 Comparative photocatalytic degradation properties of MB by P25, commercial MoO_3 and recycled MoO_3 under visible light irradiation

$$D = (D_0 - D_T) / D_0 \times 100\% \quad (5)$$

where D is the degradation efficiency and C_0 and C_t are initial and residual concentration of dyes at different times. As shown in Fig. 9, the degradation of MB by the commercial MoO_3 and P25 is 5.52% and 11.18%, after irradiating for 60 min. The degradation activity of the recycled MoO_3 at 950 °C is 99.25% which is far superior to commercial MoO_3 and P25. Inset in Fig. 9 shows the corresponding colors of MB with recycling MoO_3 , among which –30 refers to the solution before dark reaction and 0 refers to the initiation of photocatalytic reaction. Finally, the blue color solution changed to colorless within the period of 60 min. The recycling MoO_3 in this

work demonstrated a good photocatalytic activity for photodegradation of MB under visible light.

Concluding Remarks

MoO₃ was recycled from waste MoSi₂ heating elements, and the recycling MoO₃ presented good functional properties. Specifically, when the waste MoSi₂ powder calcined at 500 °C and held for 180 min, that is to say, using the pest oxidation temperature, the waste MoSi₂ transformed into the mixture of MoO₃ and SiO₂ with the maximum transformation rate. Then, the pest oxidation products were heated to specific temperature to evaporate the MoO₃. The evaporated mass was stable above 900 °C, and MoO₃ was evaporated completely from MoO₃ and SiO₂ mixture. The recycling MoO₃ demonstrated stronger photocatalytic degradation of MB up to 99.25% in visible light, which was higher than commercial MoO₃ and P25. This study proved that recycled MoO₃ with good photocatalytic degradation of MB could be effectively recovered from waste MoSi₂.

Acknowledgements This work was supported by the National Natural Science Foundation of China (51574241 and 51874305), the Swedish Foundation for Strategic Research (SSF) for Infrastructure Fellowship (RIF14-0083).

Compliance with ethical standards

Conflict of interest The authors declare no conflict of interest.

References

1. P. Feng, X. Qu, A. Farid, et al., *Rare Metals* **25**, 225 (2006).
2. Y. Jiang, D. Feng, H. Ru, et al., *Surface and Coatings Technology* **339**, 91 (2018).
3. Y. Zhang, Y. Li, C. Bai, et al., *Ceramics International* **43**, 6250 (2017).
4. A. Makris, *Industrial Heating* **61**, 46 (1994).
5. V. Bizzarri, B. Linder and N. Lindskog, *American Ceramic Society Bulletin* **68**, 1834 (1989).
6. M. Samadzadeh, C. Oprea, H. Sharif, et al., *International Journal of Refractory Metals and Hard Materials* **66**, 11 (2017).
7. D. Berztiss, R. Cerchiara and E. Gulbransen, *Materials Science and Engineering: A* **155**, 165 (1992).
8. T. Chou and T. Nieh, *Scripta Metallurgica et Materialia* **26**, 1637 (1992).
9. Z. Zaki, N. Mostafa and Y. Ahmed, *International Journal of Refractory Metals and Hard Materials* **45**, 23 (2014).
10. Y. Liu, G. Shao and P. Tsakirooulos, *Intermetallics* **9**, 125 (2001).
11. P. Feng, X. Wang, Y. He, et al., *Journal of Alloys and Compounds* **473**, 185 (2009).
12. F. Zhang, L. Zhang, A. Shan, et al., *Intermetallics* **14**, 406 (2006).
13. J. Chen, C. Li, Z. Fu, et al., *Materials Science and Engineering: A* **261**, 239 (1999).
14. S. Chevalier, F. Bernard, E. Gaffet, et al., *Materials Science Forum* **461–464**, 439 (2004).
15. S. Knittel, S. Mathieu and M. Vilasi, *Intermetallics* **18**, 2267 (2010).
16. K. Kurokawa, H. Houzumi, I. Saeki, et al., *Materials Science and Engineering: A* **261**, 292 (1999).
17. C. McKamey, P. Tortorelli, J. DeVan, et al., *Journal of Materials Research* **7**, 2747 (1992).
18. K. Yanagihara, K. Przybylski and T. Maruyama, *Oxidation of Metals* **47**, 2 (1997).
19. T. Chou and T. Nieh, *Journal of Materials Science* **29**, 2963 (1994).

20. D. Pope and R. Darolia, *Materials Research Society Bulletin* **21**, 30 (1996).
21. A. Bouzidi, N. Benramdane, H. Tabet-Derraz, et al., *Materials Science and Engineering: B* **97**, 5 (2003).
22. M. Rahmania, S. Keshmiri, J. Yu, et al., *Sensor and Actuators B* **145**, 13 (2010).
23. I. Navas, R. Vinodkumar, K. Lethy, et al., *Journal of Physics D: Applied Physics* **42**, 175305 (2009).
24. A. Chithambararaj, N. Sanjini, A. Chandra Bose, et al., *Catalysis Science & Technology* **3**, 1405 (2013).
25. V. Kumar, K. Gayathri and S. Anthony, *Materials Research Bulletin* **76**, 147 (2016).
26. S. Sunu, E. Prabhu, V. Jayaraman, et al., *Sensor and Actuators B* **94**, 189 (2003).
27. J. Zhou, S. Deng, N. Xu, et al., *Applied Physics Letters* **83**, 2653 (2003).
28. A. Prasad, P. Gouma, D. Kubinski, et al., *Thin Solid Films* **436**, 46 (2003).
29. A. Prasad, D. Kubinski and P. Gouma, *Sensors and Actuators B: Chemical* **93**, 25 (2003).
30. K. Gesheva and T. Ivanova, *Chemical Vapor Deposition* **12**, 231 (2006).
31. S. Ashraf, C. Blackman, G. Hyett, et al., *Journal of Materials Chemistry* **16**, 3575 (2006).
32. R. Patil, M. Uplane and P. Patil, *Applied Surface Science* **252**, 8050 (2006).
33. K. Hellström, P. Persson and E. Ström, *Journal of the European Ceramic Society* **35**, 513 (2015).
34. X. Liu, S. Wang, Q. Zhang, et al., *Chinese Journal of Materials Research* **24**, 17 (2010).
35. S. L. Prabavathi, P. S. Kumar, K. Saravanakumar, et al., *Journal of Photochemistry and Photobiology A* **356**, 642 (2018).
36. D. Zhou, Z. Chen, Q. Yang, et al., *Solar Energy Materials and Solar Cells* **157**, 399 (2016).

Publisher's Note Springer Nature remains neutral with regard to jurisdictional claims in published maps and institutional affiliations.